

UC Office of the President

UCOP Previously Published Works

Title

Infrared probe of the anomalous magnetotransport of highly oriented pyrolytic graphite in the extreme quantum limit

Permalink

<https://escholarship.org/uc/item/0jw3k2fb>

Journal

Physical Review B, 74(19)

ISSN

1098-0121

Authors

Li, Z Q
Tsai, S W
Padilla, W J
[et al.](#)

Publication Date

2006-11-01

Peer reviewed

Infrared probe of the anomalous magnetotransport of highly oriented pyrolytic graphite in the extreme quantum limit

Z. Q. Li,^{1,*} S.-W. Tsai,² W. J. Padilla,^{1,†} S. V. Dordevic,³ K. S. Burch,^{1,‡} Y. J. Wang,⁴ and D. N. Basov¹

¹*Department of Physics, University of California, San Diego, La Jolla, California 92093, USA*

²*Department of Physics, University of California, Riverside, California 92521, USA*

³*Department of Physics, The University of Akron, Akron, Ohio 44325, USA*

⁴*National High Magnetic Field Laboratory, Tallahassee, Florida 32310, USA*

(Received 5 September 2006; published 6 November 2006)

We present a systematic investigation of the magnetorelectance $R(\omega, B)$ of highly oriented pyrolytic graphite in magnetic field B up to 18 T. From these measurements, we report the determination of lifetimes τ associated with the lowest Landau levels in the quantum limit. We find a linear field dependence for inverse lifetime $1/\tau(B)$ of the lowest Landau levels, which is consistent with the hypothesis of a three-dimensional (3D) to 1D crossover in an anisotropic 3D metal in the quantum limit. This enigmatic result uncovers the origin of the anomalous linear in-plane magnetoresistance observed both in bulk graphite and recently in mesoscopic graphite samples.

DOI: [10.1103/PhysRevB.74.195404](https://doi.org/10.1103/PhysRevB.74.195404)

PACS number(s): 78.30-j, 71.70.Di, 72.20.My, 78.40.Kc

I. INTRODUCTION

Intense magnetic fields can radically alter properties of materials and produce a myriad of novel effects and novel states of matter.¹⁻³ One intriguing example is the field-induced transformation expected in an anisotropic three-dimensional (3D) metal. Provided only the lowest Landau levels (LLs) are populated (a condition referred to as the quantum limit), coherent charge motion in the direction perpendicular to the magnetic field is arrested. Therefore, magnetic field initiates a crossover from 3D to 1D transport along the direction of the field.⁴ A suitable candidate system to exhibit this phenomenon is graphite. In this anisotropic semimetal comprised of weakly coupled graphene sheets, a combination of low carrier density and small effective masses allows one to achieve the quantum limit condition in fairly modest magnetic fields along the c axis (7–8 T).⁵ A manifestation of the 3D to 1D crossover is the field dependence of the relaxation rate $1/\tau$ associated with the lowest LLs.⁴ This fundamental electronic characteristic is difficult to infer from transport studies but can be directly probed via infrared (IR) spectroscopy.

Here, via IR spectroscopy of graphite we probe lifetimes τ associated with the lowest LLs in the quantum limit with a field perpendicular to the graphene planes. We find that $1/\tau \propto B$ for the lowest LLs, which is distinct from power laws typically found in other classes of low dimensional systems¹ but consistent with the hypothesis of a 3D to 1D crossover.⁴ Empowered by the experimental data for lifetimes, we were able to elucidate the anomalous linear magnetoresistance in samples of weakly interacting graphene sheets. This peculiar form of magnetoresistance was discovered nearly 40 years ago in bulk graphite^{5,6} and recently observed in mesoscopic samples comprised of only a few graphene layers.⁷

II. EXPERIMENTAL METHODS

Highly oriented pyrolytic graphite (HOPG) samples studied in this work were extensively characterized through mag-

netotransport measurements.⁸ They have ab -plane surfaces with typical dimensions $6 \times 6 \text{ mm}^2$. The zero field reflectance $R(\omega)$ was measured over broad frequency (15 to 25 000 cm^{-1}) and temperature (10 to 292 K) ranges at UCSD. The complex optical conductivity $\sigma(\omega) = \sigma_1(\omega) + i\sigma_2(\omega)$ in zero field was obtained from Kramers-Kronig (KK) transformation of the reflectance data. The Hagen-Rubens formula was employed in the low ω region. KK-derived results are consistent with those obtained by ellipsometry.

The magnetorelectance $R(\omega, B)$ were measured in the Faraday geometry: \mathbf{E} vector in the graphene plane and magnetic field \mathbf{B} parallel to the c axis of the sample. Our in-house apparatus enables absolute measurements of $R(\omega, B)$ in fields up to 9 T over a broad frequency range (15 to 4000 cm^{-1}).⁹ Data in selected magnetic fields were acquired using a sub-THz Martin-Puplett interferometer and extend down to 7 cm^{-1} . The magnetorelectance ratios $R(\omega, B)/R(\omega, B=0)$ in the range 20–3000 cm^{-1} with $B=7$ –18 T were obtained at the National High Magnetic Field Laboratory in Tallahassee. All data in the magnetic field were taken at 5 K.

III. ZERO FIELD DATA

The zero field reflectance $R(\omega)$ and dissipative part of the optical conductivity $\sigma_1(\omega)$ are plotted in Fig. 1. The room temperature $R(\omega)$ spectrum is consistent with earlier studies in the overlapping frequency range.¹⁰ The $R(\omega)$ spectrum shows a typical metallic behavior: a gradual depression of reflectance with increasing frequency towards a plasma minimum at about 24 000 cm^{-1} , followed by a sharp onset due to the interband transition between π bands at the M points of the Brillouin zone.⁵ An edgelike structure in the far-IR reflectance shows an interesting temperature dependence with softening of the edge from 400 cm^{-1} at 292 K down to 200 cm^{-1} at 10 K. The zero field $\sigma_1(\omega)$ spectra are dominated by the Drude component but in addition show a sub-

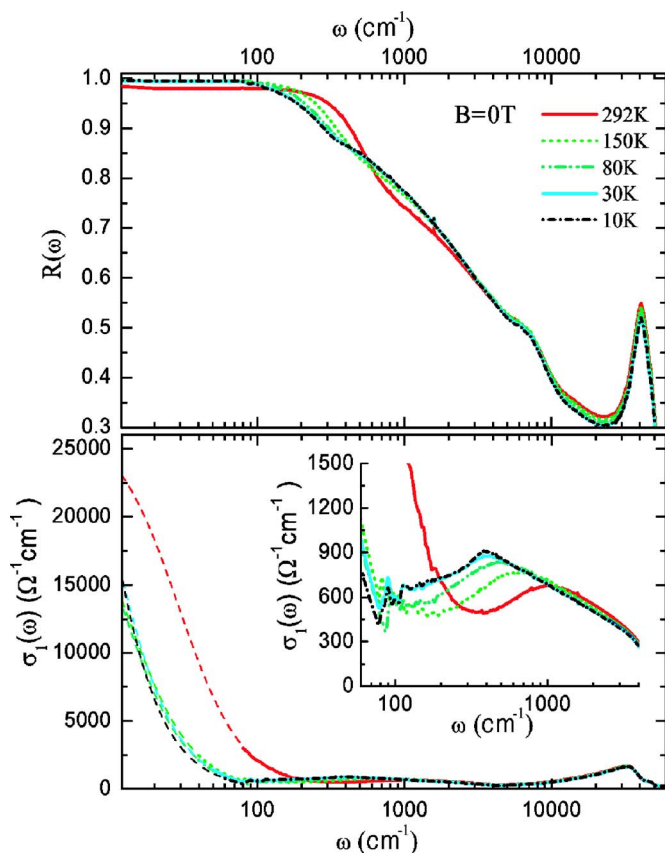


FIG. 1. (Color online) Zero field *ab*-plane reflectance $R(\omega)$ (top panel) and real part of the optical conductivity $\sigma_1(\omega)$ (bottom panel) of graphite. The thin dashed lines in the bottom panel are Drude fits of the $\sigma_1(\omega)$ spectra in the low frequency region. The bottom inset displays the absorption peak of $\sigma_1(\omega)$ in the mid-IR region, which shifts to high energy with increasing temperature.

stantial contribution throughout the mid-IR range. This is detailed in the bottom inset of Fig. 1 displaying a broad resonance corresponding to the edge observed in raw $R(\omega)$ data. As temperature is reduced the Drude mode narrowed indicative of strong depression of the quasiparticle scattering rate $1/\tau$. We also found that mid-IR resonance softens with the center peak shifting from 1000 cm^{-1} at 292 K down to 400 cm^{-1} at 10 K.

We assign the mid-IR resonance to the interband transitions between the π bands near K and H points of the Brillouin zone,⁵ as shown in Fig. 2. The conventional Slonczewski-Weiss-McClure (SWMC) band theory of graphite⁵ prescribes the following relations for the onsets of interband transitions near K and H points:¹¹ $\Delta E_K \approx 2(E_F - 2\gamma_2)$ and $\Delta E_H = \Delta - 2E_F$, where Δ and γ_2 are the band parameters. Therefore, the lowering of the Fermi energy^{5,12} and π bands near the K point⁵ with the increase of T is expected to cause hardening of the transitions at K and H points, as shown in Fig. 2. The observed trends are consistent with the depression of E_F by 40% at 292 K compared to the value at 10 K assuming accepted values for the Fermi energy and the band parameters (at 10 K): $E_F = -25 \text{ meV}$, $\Delta = 0.04 \sim 0.05 \text{ eV}$ (Ref. 13) and $\gamma_2 = -0.02 \text{ eV}$. Although this effect has not been directly observed before, the evolution of the

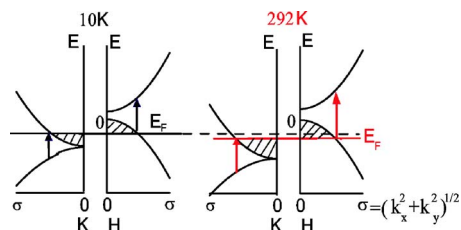


FIG. 2. (Color online) Schematics of the band structure of graphite at K and H points of the Brillouin zone at 10 and 292 K. The arrows indicate the interband transitions observed in the bottom inset of Fig. 1.

resonance structure in $\sigma_1(\omega)$ with T is in accord with the well established notion that the dominant contribution to the carrier dynamics and electrodynamics of graphite is associated with K and H points of the Brillouin zone.⁵ Therefore, our zero field results are in excellent agreement with the SWMC band model. The applicability of the SWMC model was corroborated by recent angle resolved photoemission spectroscopy studies of HOPG.¹⁴

IV. MAGNETOREFLECTANCE DATA

Insights into the anomalous magnetotransport can be provided by a systematic investigation of magnetorefectance $R(\omega, B)$ spectra, which are displayed in a ω/B scaled plot in Fig. 3. To highlight field-induced changes of the optical

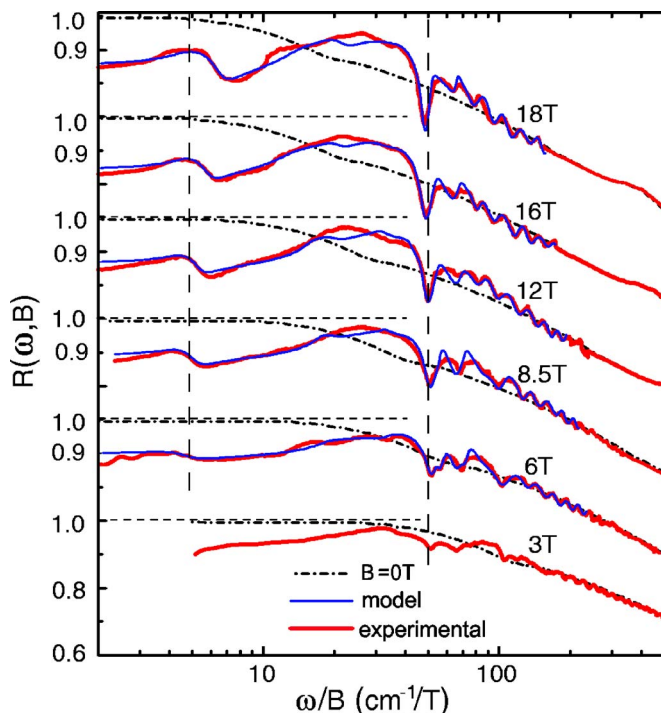


FIG. 3. (Color online) The ω/B scaled plot of the *ab*-plane reflectance spectra $R(\omega, B)$ in several magnetic fields. At each field B , the zero field reflectance spectrum $R(\omega, B=0)$ is also scaled by the corresponding factor B for comparison. Every set of spectra is offset by 30% for clarity. The model spectra are obtained from the analysis detailed in the text.

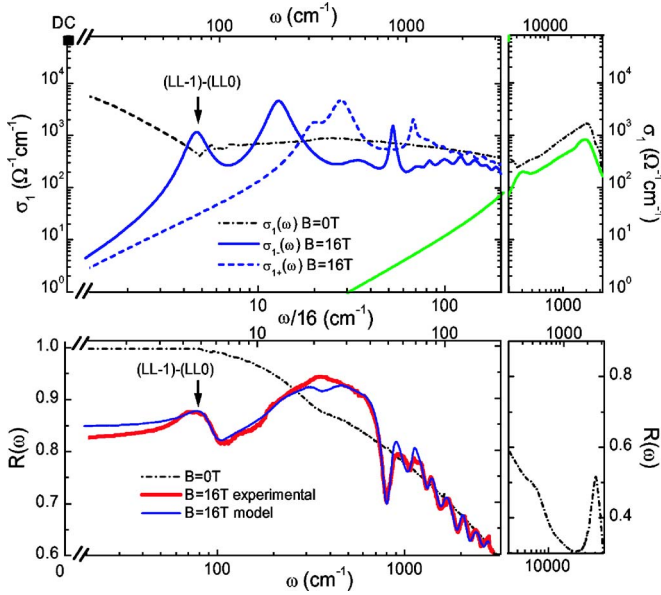


FIG. 4. (Color online) Top panel: $\sigma_1(\omega)$ at zero field and model spectra $\sigma_{1+}(\omega)$ and $\sigma_{1-}(\omega)$ at 16 T obtained from the analysis detailed in the text. The black square on the left axis represents the dc conductivity σ_{dc} at 0 T. The green (light gray) curve is the high frequency field-independent absorption in both $\sigma_{1-}(\omega)$ and $\sigma_{1+}(\omega)$. Bottom panel: experimental $R(\omega)$ spectra at 0 and 16 T and model spectra $R(\omega)$ at 16 T. The arrows indicate the resonance features in $R(\omega)$ and $\sigma_{1-}(\omega)$ due to the (LL-1)-(LL0) transition.

properties, at each field B the zero field reflectance spectrum $R(\omega, B=0)$ is also scaled by the same factor B and shown together with $R(\omega, B)$ for comparison. Two features are observed in the high-field spectra: (i) the reflectance at low frequency is strongly suppressed and no longer extrapolates to unity in the limit of $\omega \rightarrow 0$; (ii) the $R(\omega, B)$ spectra reveal a series of field-dependent resonances extending up to 3000 cm^{-1} (see also the bottom panel of Fig. 4). The dramatic suppression of the low frequency reflectance $R(\omega \rightarrow 0, B)$ is an IR counterpart of the enormous positive magnetoresistance of graphite exceeding 10^3 in 18 T field.⁵ The resonance features in $R(\omega, B)$ originate from the inter-LL transitions. An inspection of Fig. 3 shows that the frequencies of the strongest resonances reveal a linear dependence on magnetic field.

The rather complicated form of the $R(\omega, B)$ spectra and its systematic evolution with magnetic field are both in accord with the SWMC band theory of HOPG. To show this we analyzed $R(\omega, B)$ spectra displayed in Fig. 3 using a magneto-optical Lorentzian model for the complex conductivity due to inter-LL transitions $\sigma_{\pm}^{LL}(\omega)$:¹⁵

$$\sigma_{\pm}^{LL}(\omega) = \sum_j \frac{\omega_{pj\pm}^2}{4\pi} \frac{\omega}{\omega/\tau_{j\pm} + i(\omega_{j\pm}^2 - \omega^2)}. \quad (1)$$

This equation yields a series of resonance peaks at ω_{j+} and ω_{j-} at the poles of the left- and right-hand circularly polarized conductivity $\sigma_{\pm}^{LL}(\omega)$. Each peak is defined through the linewidth $1/\tau_{j\pm}$ and the oscillator strength $\omega_{pj\pm}^2$. Inter-LL transitions at both K and H points of the Brillouin zone^{16,17}

are included in our fitting. According to SWMC theory, more than a dozen inter-LL transitions are likely to contribute to $R(\omega, B)$ in the studied frequency range. However, the parameters in Eq. (1) are strictly constrained by both the analytical properties of $\sigma_{\pm}(\omega)$ (Ref. 15) and the selection rules of inter-LL transitions.^{5,17} Following these constraints, Eq. (1) is used to construct $\sigma_{+}(\omega)$ and $\sigma_{-}(\omega)$, which are then used to evaluate the reflectance spectra $R(\omega) = \frac{1}{2}[R_{+}(\omega) + R_{-}(\omega)]$. In addition, several field-independent Lorentzian oscillators are employed in both $\sigma_{1+}(\omega)$ and $\sigma_{1-}(\omega)$ to account for the absorption above 3000 cm^{-1} , as displayed by the green (light gray) curve in Fig. 4. We observed an additional resonance feature in $R(\omega, B)$ below 8.5 T in the range $50\text{--}100 \text{ cm}^{-1}/\text{T}$ in Fig. 3, which is an expected consequence of the quantum limit.¹⁸ The resonances in $R(\omega, B)$ below and above 8.5 T are roughly at the same positions in the ω/B plot, with small deviations in the high frequency resonances. The two different sets of magneto-optical oscillators at $\omega_{j\pm}/B$ employed to fit experimental $R(\omega, B)$ are summarized in Table I. We use the transition energies from Ref. 17 to account for the inter-LL transitions at the H point. These transitions are at much higher energy compared to those at the K point and constitute a broad background in $R(\omega, B)$ spectra.¹⁷ We stress that all field-dependent oscillators employed in our model can be assigned to the inter-LL transitions at K and H points within the conventional SWMC band model.⁵

The model spectra at representative fields obtained from the above analysis are depicted in Figs. 3 and 4. Both the peak structures and their field dependence in experimental $R(\omega, B)$ spectra are reproduced by our analysis. Of special interest is the lowest inter-LL transition (LL-1)-(LL0) shown in Fig. 5. This transition is well separated from higher energy resonances, therefore the reflectance in the vicinity of this mode is hardly affected by other higher energy modes in our model, which allows us to extract the parameters for this particular transition from the above analysis. Moreover, in the quantum limit LL-1 and LL0 are the only occupied levels,⁵ which are directly related to the magnetotransport properties. Therefore, special attention will be given to the (LL-1)-(LL0) transition. Both the resonance frequency of this transition and its linewidth $1/\tau$ follow a linear field dependence as shown in Fig. 5. This is evident from a close inspection of the experimental $R(\omega, B)$ spectra in Fig. 3. The power law of $1/\tau(B)$ below 6 T field is yet to be explored, because at low fields the (LL-1)-(LL0) transition occurs at low energies beyond our detection limit.

V. DISCUSSION

Our magnetorefectance data are in accord with the conventional SWMC band model of graphite.⁵ In the SWMC model, the inter-LL transitions at K and H points have different field dependence: transitions at the K point reveal “normal” quasiparticle behavior (linear B scaling),⁵ whereas transitions at the H point show Dirac behavior at high fields ($\sim\sqrt{B}$ scaling).¹⁷ Inter-LL transitions at both K and H points of the Brillouin zone are needed to fully account for our results on HOPG, which is consistent with a previous

TABLE I. The magneto-optical Lorentzian oscillators used in the analysis of $R(\omega, B)$ and their possible assignments. ω_+/B and ω_-/B (in cm^{-1}/T) are frequencies (normalized by magnetic field B) of the oscillators in $\sigma_+(\omega)$ and $\sigma_-(\omega)$, respectively, used to account for the inter-Landau-level (LL) transitions at K point. Two sets of oscillators are used in two field ranges: (*h*) $B > 8.5$ T and (*l*) $B \leq 8.5$ T. The theoretical transition frequencies are labeled following Nakao's notation (Ref. 16): *hn-em* refers to the transition from the n th hole LL to the m th electron LL, etc. The transitions *e1-e8* and *e1-e9* are allowed only below the quantum limit. The last eight columns list $\omega_{pj\pm}$ and $1/\tau_{j\pm}$ (both in cm^{-1}) used for the model spectrum $R(\omega)$ at 16 and 8.5 T. The parameters of the oscillator used for $m^+ = 0, -1$ transitions at H point are 16 T: $\omega_0 = 1212 \text{ cm}^{-1}$, $\omega_p = 4243 \text{ cm}^{-1}$, $1/\tau = 500 \text{ cm}^{-1}$; 8.5 T: $\omega_0 = 818 \text{ cm}^{-1}$, $\omega_p = 3211 \text{ cm}^{-1}$, $1/\tau = 300 \text{ cm}^{-1}$.

ω_-^h/B	ω_-^l/B	Theory	Assignment	ω_+^h/B	ω_+^l/B	Theory	Assignment	$\omega_{pj-}^{16 \text{ T}}$	$\omega_{pj+}^{16 \text{ T}}$	$1/\tau_{j-}^{16 \text{ T}}$	$1/\tau_{j+}^{16 \text{ T}}$	$\omega_{pj-}^{8.5 \text{ T}}$	$\omega_{pj+}^{8.5 \text{ T}}$	$1/\tau_{j-}^{8.5 \text{ T}}$	$1/\tau_{j+}^{8.5 \text{ T}}$
4.6	4.3	4.5	(LL-1)-(LL0)	19.7	19.3	22	(LL-1)-e1	1238	2265	10	40	725	1347	6	24
13	18	17	(LL0)-e1	28	33	35	(LL0)-e2	4016	5578	29	60	3683	4953	5	10
35	35	32	<i>h2</i> -(LL0)	50	50	49	<i>h2</i> -e1	2079	2377	167	227	2325	2629	96	128
54		54	<i>h1</i> -e2	69		70	<i>h1</i> -e3	2082	2349	26	33				
	58	58	<i>h3</i> -e1		73	70	(LL-1)-e4					1959	2130	7	9
70	61	66	(LL0)-e4	85	76	76	<i>h3</i> -e2	1538	1672	146	175	1581	1753	36	45
						81	(LL0)-e5								
83	80	84	<i>h2</i> -e3	98	95	98	<i>h2</i> -e4	1056	1143	67	78	2340	2519	92	108
		85	<i>h4</i> -e2			101	<i>h4</i> -e3								
100		99	<i>h1</i> -e5	115		113	<i>h1</i> -e6	2461	2615	210	240				
	111	105	<i>e1</i> -e8		126	119	<i>e1</i> -e9					2158	2293	70	79
		107	<i>h3</i> -e4			121	<i>h3</i> -e5								
		110	<i>h5</i> -e3			124	<i>h5</i> -e4								
122		127	<i>h2</i> -e6	137		141	<i>h2</i> -e7	1874	1977	128	143				
		130	<i>h4</i> -e5			144	<i>h4</i> -e6								
	141	141	<i>h1</i> -e8		156	155	<i>h1</i> -e9					2213	2324	73	80
145		149	<i>h3</i> -e7	160		163	<i>h3</i> -e8	2305	2409	211	232				
		153	<i>h5</i> -e6			167	<i>h5</i> -e7								
	164	169	<i>h2</i> -e9		179	183	<i>h2</i> -e10					2343	2442	101	110
167		172	<i>h4</i> -e8	182		186	<i>h4</i> -e9	1498	1559	172	187				
		175	<i>h6</i> -e7			189	<i>h6</i> -e8								

magneto-optical study of bulk graphite samples.¹⁷ Recently, inter-LL transitions with \sqrt{B} scaling were observed in a magnetotransmission study of ultrathin graphite layers,¹⁹ which may come from transitions at the H point due to interlayer coupling between graphene sheets.

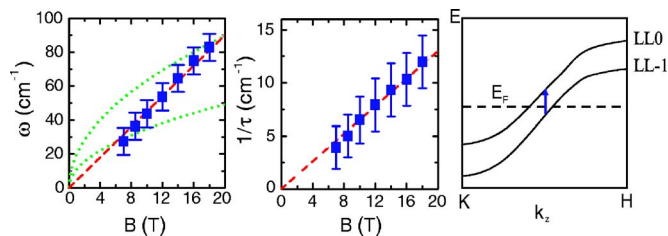


FIG. 5. (Color online) Resonance frequency (left panel) and linewidth (middle panel) of the (LL-1)-(LL0) transition in magnetic field. The dashed curves in these two panels are linear fits to the data. The dotted curves in the left panel are $\omega \sim \sqrt{B}$ fits. Right panel: a schematic of the LL-1 and LL0 Landau levels in the quantum limit (adapted from Ref. 25).

We now show that the observed $1/\tau \propto B$ dependence for the (LL-1)-(LL0) transition (Fig. 5) is consistent with the notion of 3D to 1D crossover in an anisotropic 3D metal in the quantum limit.⁴ The $1/\tau \propto B$ behavior in Fig. 5 most likely originates from the linear field dependence of the broadening of both LL-1 and LL0,²⁰ which defines the scattering rate of the quasiparticles associated with these levels. In the quantum limit, the carriers have finite momentum only along the field direction (c axis) and move diffusively in the transverse direction (ab plane) when scattered by impurities. The carrier-impurity scattering rate $1/\tau$ in the quantum limit is given by $1/\tau(B) = 2\pi n_0 u_0^2 \nu_B$,⁴ where the density of neutral impurities n_0 and impurity potential u_0 are B independent. The 3D density of states ν_B increases linearly with B in the quantum limit in graphite,⁵ giving rise to the linear B dependence of $1/\tau$. The increase of $1/\tau$ by a factor of 3 from 6 T to 18 T is consistent with a threefold increase of ν_B in this range.⁵ The interactions between carriers can give additional corrections to $1/\tau(B)$, which have weak logarithmic field dependence.²¹ Therefore, our data for the field dependence of the relaxation rate are in accord with the specific prediction

of a model involving 3D to 1D crossover in the quantum limit.

Based on the observed $1/\tau \propto B$ result, we propose an explanation for the anomalous linear magnetoresistance found both in mesoscopic graphite systems⁷ and in bulk graphite.⁵ First, the giant positive magnetoresistance of graphite is clearly related to the electronic spectral weight transfer of the Drude mode in the $B=0$ spectrum to finite energies in magnetic field (Fig. 4). The spectral weight transfer results in a drastic suppression of the conductivity in the $\omega \rightarrow 0$ limit by more than 10^3 . Data in Figs. 3 and 4 furthermore show that the lowest energy electronic excitation in the quantum limit is the (LL-1)-(LL0) transition revealing the linear field dependence of the relaxation rate. Let us explore the consequences of these findings for magnetoresistance that we will analyze following the standard form appropriate for the quantum limit as shown in,^{4,22}

$$\rho_{xx} = \frac{\rho_1 \rho_2 (\rho_1 + \rho_2) + (\rho_1 R_2^2 + \rho_2 R_1^2) B^2}{(\rho_1 + \rho_2)^2 + (R_1 + R_2)^2 B^2}, \quad (2)$$

where ρ_{xx} is the ab -plane resistivity, ρ_i and $R_i = 1/n_i q_i$ are the resistivity and Hall coefficient of the electrons ($i=1$) and holes ($i=2$), and n_i and q_i are the density and charge of the carriers. Note that in the quantum limit the off-diagonal term in the resistivity tensor can still be expressed as $R_i B$ as shown in Ref. 4. We emphasize that here Eq. (2) follows from a fully quantum mechanical treatment yielding the magnetic field dependence of ρ_i and R_i . This is distinct from the semiclassical model of magnetoresistance, in which ρ_i and R_i are constants. At high fields, the B^2 term dominates over the zero field term in the numerator; therefore, the latter can be neglected. In the quantum limit, transport in the ab plane is diffusive with ρ_i given by $1/\rho_i \sim e^2 \nu_B D_i$,²¹ where $D \sim l_B^2/\tau$ is the diffusion coefficient and $l_B = 1/\sqrt{eB}$ is the magnetic length. From $\nu_B \propto B$,⁵ and $D \sim l_B^2/\tau \propto B/B \sim 1$ ($1/\tau \propto B$ from our results), we obtain $1/\rho_i \propto B$. Because the net carrier density in the sample $n_1 - n_2$ is constant at high field^{5,23} and $n_1 \approx n_2 \propto B$, we obtain $(R_1 + R_2)B = [(n_1 - n_2)/n_1 n_2 e]B \propto 1/B$. This expression is valid in the magnetic field regime where graphite shows linear magnetoresistance. In even higher field, $n_1 - n_2$ decreases with field due to the so-called magnetic freeze-out effect, and correspondingly a saturation of magnetoresistance is observed.²³ Combined with $R_i = 1/n_i e \propto 1/B$, we find $\rho_{xx} \propto B$. Therefore, our study suggests that the anomalous linear magnetoresistance of graphite originates from quantum transport in magnetic field. The above analysis can also be used to account for the linear

magnetoresistance in mesoscopic graphite-based electronic systems,⁷ where interlayer coupling between graphene sheets is important.

The use of a two-band model in our analysis is corroborated by a recent study of mesoscopic graphite field-effect transistors,⁷ which shows that the slope of the magnetoresistance can be tuned by changing the carrier compensation $n_e - n_h$ consistent with Eq. (2). Previously, a model based on magnetic-field-dependent scattering range of ionized impurity scattering⁶ was proposed to explain the linear magnetoresistance in graphite. Due to the field-dependent screening of charged impurities, the scattering rate in this model has a field dependence of $1/\tau \sim B/(c+B)^2$, where c is a constant.⁶ This prediction is in contrast to our observation $1/\tau \propto B$. Therefore, our study shows that impurities in graphite are likely to be uncharged and the ionized impurity scattering model⁶ may not be applicable. Indeed, previous magnetotransport studies have shown the limitations of the ionized impurity model.^{24,25} Recently, an interesting model based on Dirac fermions²⁶ is proposed to account for linear magnetoresistance in graphite. However, our studies of HOPG have clearly demonstrated that Dirac fermions do not play a dominant role in the magnetotransport in graphite.

VI. SUMMARY

In this study, we carried out systematic IR magneto-optical experiments on HOPG. We show that the optical properties of HOPG in both zero field and magnetic fields can be understood within the conventional SWMC band theory of graphite.⁵ We observed an unconventional linear field dependence of the inverse lifetime $1/\tau$ associated with the lowest LLs. This observation is consistent with the hypothesis of 3D to 1D crossover in an anisotropic 3D metal in the quantum limit.⁴ This result has allowed us to address the origin of the anomalous linear magneto-resistance in mesoscopic graphite-based electronic systems⁷ as well as in bulk graphite.⁵ Our work has demonstrated the potential of IR spectroscopy for the study of LL dynamics and novel magnetotransport phenomena in carbon based materials such as mesoscopic graphite and graphene,^{27,28} which are directly related to the novel functionalities of magnetoelectronic devices based on these materials.

ACKNOWLEDGMENTS

This work was supported by the DOE and NSF. We thank P. Esquinazi for providing samples.

*Electronic address: zhiqiang@physics.ucsd.edu

†Present address: Department of Physics, Boston College, Chestnut Hill, MA 02467.

‡Present address: Los Alamos National Laboratory, MS K771, MPA-CIN, Los Alamos, NM 87545.

¹T. Ando, A. B. Fowler, and F. Stern, Rev. Mod. Phys. **54**, 437 (1982).

²S. Das Sarma and A. Pinczuk, *Perspectives in Quantum Hall Effects* (John Wiley & Sons, New York, 1997).

³D. N. Basov and T. Timusk, Rev. Mod. Phys. **77**, 721 (2005).

⁴A. A. Abrikosov, Sov. Phys. JETP **29**, 746 (1969).

⁵N. B. Brandt, S. M. Chudinov, and Ya. G. Ponomarev, *Semimetals: 1. Graphite and its Compounds* (Elsevier Science, New York, 1988).

- ⁶J. W. McClure and W. J. Spry, *Phys. Rev.* **165**, 809 (1968).
- ⁷Yuanbo Zhang, Joshua P. Small, Michael E. S. Amori, and Philip Kim, *Phys. Rev. Lett.* **94**, 176803 (2005); S. V. Morozov, K. S. Novoselov, F. Schedin, D. Jiang, A. A. Firsov, and A. K. Geim, *Phys. Rev. B* **72**, 201401 (2005).
- ⁸Y. Kopelevich, P. Esquinazi, J. H. S. Torres, R. R. da Silva, and H. Kempa, *Adv. Solid State Phys.* **43**, 207 (2003).
- ⁹W. J. Padilla, Z. Q. Li, K. S. Burch, Y. S. Lee, K. J. Mikolaitis, and D. N. Basov, *Rev. Sci. Instrum.* **75**, 4710 (2004).
- ¹⁰D. L. Greenaway, G. Harbeke, F. Bassani, and E. Tosatti, *Phys. Rev.* **178**, 1340 (1968); E. A. Taft and H. R. Phillipp, *Phys. Rev.* **138**, A197 (1965).
- ¹¹From the expressions and structures of the four π bands in the SWMC model (see Ref. 5), the onset energy of interband transitions at K and H points can be calculated using the particular values of parameters at these points.
- ¹²I. L. Spain, *J. Chem. Phys.* **52**, 2763 (1970); L. C. Olsen, *Phys. Rev. B* **6**, 4836 (1972).
- ¹³This value of Δ agrees with the value from an early optical study: G. Guizzetti, L. Nosenzo, E. Reguzzoni, and G. Samoggia, *Phys. Rev. Lett.* **31**, 154 (1973); G. Bellodi, A. Borghesi, G. Guizzetti, L. Nosenzo, E. Reguzzoni, and G. Samoggia, *Phys. Rev. B* **12**, 5951 (1975), but it is somehow higher than the values in the literature obtained from other techniques.
- ¹⁴S. Y. Zhou, G.-H. Gweon, and A. Lanzara, *Ann. Phys. (N.Y.)* **321**, 1730 (2006).
- ¹⁵B. Lax and J. G. Mavroides, in *Semiconductors and Semimetals Vol. 3*, edited by R. K. Willardson and A. C. Beer (Academic Press, New York and London, 1967), pp. 321–401. There are strict constraints between ω_{j+} and ω_{j-} , $1/\tau_{j+}$ and $1/\tau_{j-}$, as well as ω_{pj+}^2 and ω_{pj-}^2 , because by definition $\sigma_+(\omega)$ and $\sigma_-(\omega)$ are related by $\sigma_{\pm}(\omega) = \sigma_{xx}(\omega) \pm i\sigma_{xy}(\omega)$.
- ¹⁶K. Nakao, *J. Phys. Soc. Jpn.* **40**, 761 (1976).
- ¹⁷W. W. Toy, M. S. Dresselhaus, and G. Dresselhaus, *Phys. Rev. B* **15**, 4077 (1977).
- ¹⁸The different resonance features below and in the quantum limit can be attributed to the different allowed inter-LL transitions in these two ranges. For instance, the inter-LL transitions such as $e1-e8$ and $e1-e9$ are only allowed below the quantum limit, as detailed in Table I.
- ¹⁹M. L. Sadowski, G. Martinez, M. Potemski, C. Berger, and W. A. de Heer, cond-mat/0605739 (unpublished).
- ²⁰In 2D systems under strong magnetic field, the resonance line-width of the inter-LL transition coincides with the broadening of the corresponding LLs, provided impurity scattering is the dominant relaxation process (Ref. 1).
- ²¹S.-W. Tsai, D. L. Maslov, and L. I. Glazman, *Physica B* **312**, 586 (2002).
- ²²N. W. Ashcroft and N. D. Mermin, *Solid State Physics* (Holt, Rinehart and Winston, New York, 1976).
- ²³N. B. Brandt, G. A. Kapustin, V. G. Karavaev, A. S. Kotosonov, and E. A. Svistova, *Zh. Eksp. Teor. Fiz.*, **67**, 1136 (1974) [*Sov. Phys. JETP* **40**, 564 (1975)].
- ²⁴Y. Iye, P. M. Tedrow, G. Timp, M. Shayegan, M. S. Dresselhaus, G. Dresselhaus, A. Furukawa, and S. Tanuma, *Phys. Rev. B* **25**, 5478 (1982).
- ²⁵Y. Iye, L. E. McNeil, and G. Dresselhaus, *Phys. Rev. B* **30**, 7009 (1984).
- ²⁶A. A. Abrikosov, *Phys. Rev. B* **60**, 4231 (1999).
- ²⁷N. M. R. Peres, F. Guinea, and A. H. Castro Neto, *Phys. Rev. B* **73**, 125411 (2006); Johan Nilsson, A. H. Castro Neto, F. Guinea, N. M. R. Peres, cond-mat/0607343 (unpublished).
- ²⁸V. P. Gusynin, S. G. Sharapov, and J. P. Carbotte, *Phys. Rev. Lett.* **96**, 256802 (2006); cond-mat/0607727 (unpublished).